Geophysical Journal International

Geophys. J. Int. (2019) **217,** 2021–2034
Advance Access publication 2019 March 11
GJI Seismology

doi: 10.1093/gji/ggz132

A discrete representation of a heterogeneous viscoelastic medium for the finite-difference modelling of seismic wave propagation

Jozef Kristek,[1,2] Peter Moczo,[1,2] Emmanuel Chaljub[3,4] and Miriam Kristekova[1,2]

[1] *Faculty of Mathematics, Physics and Informatics, Comenius University Bratislava, Mlynska dolina F1,* 84248 *Bratislava, Slovak Republic. E-mail: kristek@fmph.uniba.sk*
[2] *Earth Science Institute, Slovak Academy of Sciences, Dubravska cesta* 9, 84528 *Bratislava, Slovak Republic*
[3] *Univ. Grenoble Alpes, ISTerre, F-*38041 *Grenoble, France*
[4] *CNRS, ISTerre, F-*38041 *Grenoble, France*

Accepted 2019 March 9. Received 2019 February 15; in original form 2018 November 16

SUMMARY

The accuracy and efficiency of numerical simulations of seismic wave propagation and earthquake ground motion in realistic models strongly depend on discrete grid representation of the material heterogeneity and attenuation. We present a generalization of the orthorhombic representation of the elastic medium to the viscoelastic medium to make it possible to account for a realistic attenuation in a heterogeneous viscoelastic medium with material interfaces. An interface is represented by an averaged orthorhombic medium with rheology of the Generalized Maxwell body (GMB-EK, equivalent to the Generalized Zener body). The representation is important for the possibility of applying one explicit finite-difference scheme to all interior grid points (points not lying on a grid border) no matter what their positions are with respect to the material interface. This is one of the key factors of the computational efficiency of the finite-difference modelling. Smooth or discontinuous heterogeneity of the medium is accounted for only by values of the effective (i.e. representing reasonably averaged medium) grid moduli and densities. Accuracy of modelling thus very much depends on how the medium heterogeneity is represented/averaged. We numerically demonstrate accuracy of the developed orthorhombic representation. The orthorhombic representation neither changes the structure of calculating stress-tensor components nor increases the number of arithmetic operations compared to a smooth weakly heterogeneous viscoelastic medium. It is applicable to the velocity–stress, displacement–stress and displacement FD schemes on staggered, partly staggered, Lebedev and collocated grids. We also present an optimal procedure for a joint determination of the relaxation frequencies and anelastic coefficients.

Key words: Numerical approximations and analysis; Computational seismology; Earthquake ground motions; Theoretical seismology; Wave propagation.

1 INTRODUCTION

The realistic physical model of a medium has to be sufficiently accurately and efficiently represented by a discrete grid model in the numerical modelling of seismic wave propagation and earthquake ground motion by the (spatial) domain numerical methods such as the finite-difference (FD) method. The possibility of applying one explicit FD scheme to all interior grid points (points not lying on a grid border), no matter what their positions are with respect to the material interface or strong material heterogeneity, is one of the key factors of the computational efficiency of the FD modelling. Smooth or discontinuous heterogeneity of the medium is accounted for only by values of the effective grid moduli and densities. Consequently, accuracy of the FD modelling very much depends on how these effective grid parameters are evaluated. With a proper discrete representation of material heterogeneity the most advanced FD schemes can be more efficient in case of local surface sedimentary structures than the spectral-element (SEM) and discontinuous-Galerkin methods (see, e.g. Chaljub *et al.* 2010, 2015; Maufroy *et al.* 2015).

Kristek *et al.* (2017) presented an orthorhombic representation of an elastic heterogeneous medium. They numerically demonstrated its superior accuracy. Compared to the harmonic-averaging representation (Moczo *et al.* 2002) the orthorhombic representation is more accurate mainly in the case of strong surface waves that are especially important in local surface sedimentary basins. The representation is capable of subcell resolution and 'sensing' an arbitrary shape and position of the interface in the grid.

A similar approach with a remarkable accuracy and subcell resolution has been developed also for the poroelastic media (Moczo *et al.* 2018).

The orthorhombic representation is applicable to modelling seismic wave propagation and earthquake motion in elastic media with material interfaces and smooth heterogeneities using velocity–stress, displacement–stress and displacement FD schemes on staggered, partly staggered, Lebedev and collocated grids.

In this paper, we present a generalization of the orthorhombic representation of the elastic medium to the viscoelastic medium to make it possible to account for a realistic attenuation.

There has been a significant development of methodology of incorporating realistic attenuation in the time-domain numerical methods since the pioneering contributions by Liu *et al.* (1976), Day & Minster (1984), Emmerich & Korn (1987) and Carcione *et al.* (1988). The most recent reviews of this development are provided, for example in articles by Petersson & Sjögreen (2012) and Blanc *et al.* (2016), and books by Moczo *et al.* (2014) and Carcione (2015). Therefore, we will not repeat the historical overview here. However, given the topic of this article, we regretfully cannot avoid mentioning that these reviews (except the one by Moczo *et al.*) omit material-independent memory variables. Day (1998) introduced a coarse graining (i.e. coarse spatial sampling) of the memory variables to reduce computer memory requirements. Kristek & Moczo (2003) demonstrated that it is necessary to introduce material-independent memory variables if the coarse graining should be sufficiently accurate in case of a strong material heterogeneity or interface. Another aspect important for this article is the equivalence of two alternative rheologies—the generalized Maxwell body as defined by Emmerich & Korn (1987) and the generalized Zener body—shown by Moczo & Kristek (2005). (This equivalence is missing in the recent edition of a comprehensive Carcione's book.)

In this paper, we first briefly overview the stress-strain relations for 1-D problem: a smooth heterogeneous elastic medium, smooth heterogeneous viscoelastic medium, averaged elastic medium and averaged viscoelastic medium. The brief overview explains the essence of generalizations from the elasticity to viscoelasticity and from the smooth heterogeneity to averaged medium (representing both continuous and discontinuous heterogeneity). Then we briefly recall the orthorhombic representation of the heterogeneous elastic medium. We continue with generalization of the representation to the viscoelastic medium. Further we present an optimal procedure for a joint determination of the anelastic coefficients and relaxation frequencies. Eventually we demonstrate the accuracy of the new representation using numerical tests.

2 BRIEF OVERVIEW OF THE STRESS–STRAIN RELATIONS FOR A 1-D PROBLEM

Before we present the discrete representation for the viscoelastic medium in 3-D, we briefly summarize the logic of generalizations from the elastic medium to the viscoelastic one, and from the smoothly heterogeneous medium to the averaged medium—as symbolically illustrated by Fig. 1. Though simple in 1-D, the summary given in Sections 2.1 and 2.2 is important for understanding the stress–strain relation for an averaged viscoelastic medium in a 3-D problem.

Let σ and ε be stress and strain, respectively, t time, ω frequency, M modulus, M_U unrelaxed modulus, $M(t)$ and $M(\omega)$ viscoelastic

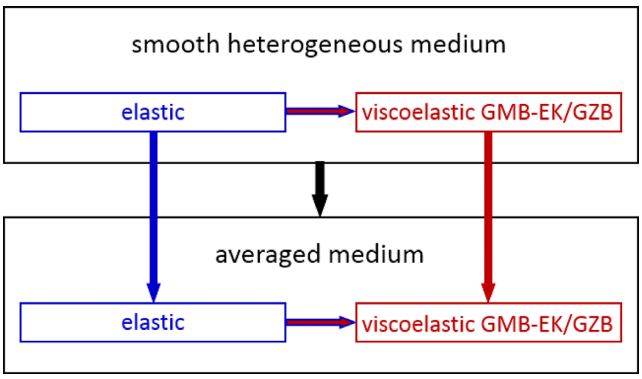

Figure 1. Scheme of generalizations: from a smoothly heterogeneous medium to an averaged medium, from an elastic medium to a viscoelastic medium.

modulus as a function of time and frequency, respectively, ζ_l and Y_l^M anelastic functions (memory variables) and anelastic coefficients, respectively, ω_l lth relaxation frequency and $Q_M(\omega)$ quality factor. GMB-EK refers to the generalized Maxwell body in definition by Emmerich and Korn (1987), and GZB refers to the generalized Zener body (see, e.g. Moczo *et al.* 2014 for the basic theory and equivalence of GMB-EK and GZB).

2.1 Smooth heterogeneous medium

Elastic medium

The time-domain stress–strain relation with the elastic modulus M is

$$\sigma(t) = M\varepsilon(t) \tag{2.1}$$

and the corresponding frequency-domain relation is

$$\sigma(\omega) = M\varepsilon(\omega). \tag{2.2}$$

In relation to viscoelasticity, the real, frequency and time independent elastic modulus may be also called the unrelaxed modulus, $M = M_U$, although there is no stress relaxation in the (perfectly) elastic medium.

Viscoelastic medium

The simple time-domain stress–strain relation (2.1) is generalized to the convolutional relation

$$\sigma(t) = M(t) * \varepsilon(t) \tag{2.3}$$

in order to account for the memory effect, and thus frequency-domain stress–strain relation (2.2) is generalized to

$$\sigma(\omega) = M(\omega)\varepsilon(\omega) \tag{2.4}$$

in which a complex-valued frequency-dependent modulus appears.

If we assume a rheology of the GMB-EK/GZB body, the viscoelastic modulus may be written as

$$M(\omega) = M_U\left[1 - \sum_{l=1}^{n} Y_l^M \frac{\omega_l}{\omega_l + i\,\omega}\right] \tag{2.5}$$

and the unrelaxed (elastic) response is quantified by the unrelaxed modulus M_U

$$M_U = \lim_{\omega\to\infty} M(\omega). \tag{2.6}$$

	ω_l	Y_l^{M,Q_1}	Y_l^{M,Q_2}
log-spaced	0.100	-0.0193	0.0135
	0.464	0.1453	0.0090
	2.154	-0.0404	0.0090
	10.000	0.8706	0.0141
minimization	0.100	0.0276	0.0147
	0.624	0.0559	0.0101
	3.210	0.1171	0.0105
	26.037	0.7861	0.0185

Figure 2. Test 1: Comparison of the relaxation frequencies ω_l and anelastic coefficients Y_l^M determined using the log-spaced approach and system of eqs (2.8) with those obtained by the minimization approach explained in Section 5.

The anelastic coefficient $Y_l^M$is defined as

$$Y_l^M = \frac{M_l}{M_U}, \tag{2.7}$$

where M_l is the elastic modulus of the lth Maxwell body in GMB-EK (see, e.g. Moczo *et al.* 2014). The anelastic coefficients may be determined from

$$\frac{1}{Q_M(\omega)} \equiv \frac{\mathrm{Im}M(\omega)}{\mathrm{Re}M(\omega)} = \frac{\sum_{l=1}^{n} Y_l^M \frac{\omega_l\,\omega}{\omega_l^2+\omega^2}}{1-\sum_{l=1}^{n} Y_l^M \frac{\omega_l^2}{\omega_l^2+\omega^2}} \tag{2.8}$$

if we know $Q_M(\omega)$. Considering, for example, Q_M values at frequencies $\tilde{\omega}_k$, a system of eq. (2.8), one equation for each $Q_M(\tilde{\omega}_k)$, is obtained. The system can be solved for the anelastic coefficients, for example using the least-square method if the number of frequencies $\tilde{\omega}_k$ is larger than the number of frequencies ω_l.

We may note that relation (2.8) simplifies if $Q >> 1$ and the attenuation mechanisms may be split into a part which could be the same over the model (time/frequency dependence) and an attenuation coefficient (spatial dependence). See the article by Yang *et al.* (2016).

Because $M(\omega)$ may be expressed in the form of a rational function of ω, it is possible to replace the convolutional relation (2.3) by a simpler form of the stress–strain relation with memory variables plus a system of additional ordinary differential equations for anelastic functions (Day & Minster 1984). For the material-independent anelastic functions (Kristek & Moczo 2003) we have

$$\sigma(t) = M_U \varepsilon(t) + \sum_{l=1}^{n} Y_l^M M_U\, \zeta_l(t) \tag{2.9}$$

$$\frac{\partial}{\partial t}\zeta_l(t) + \omega_l \zeta_l(t) = \omega_l \varepsilon(t), \quad l = 1, ..., n, \tag{2.10}$$

where n is the number of the relaxation frequencies. Summation convention does not apply to index l in eq. (2.10).

2.2 Averaged medium

Elastic medium

Consider, in general, both smooth and discontinuous heterogeneities of the elastic medium. It is then reasonable to assume some spatial averaging of the elastic modulus—for example, for an eventual discrete grid representation of the heterogeneity. Then modulus $M = M_U$ in relations (2.1) and (2.2) is replaced by a spatially averaged modulus $\bar{M} = \bar{M}_U$.

Viscoelastic medium

Analogously, moduli $M(t)$ and $M(\omega)$ are replaced by spatially-averaged moduli $\bar{M}(t)$ and $\bar{M}(\omega)$ in relations (2.3) and (2.4), respectively. If we assume that the spatially averaged viscoelastic medium can be described using the GMB-EK/GZB rheology, the averaged viscoelastic modulus may be written as

$$\bar{M}(\omega) = \bar{M}_U \left[1 - \sum_{l=1}^{n} Y_l^{\bar{M}} \frac{\omega_l}{\omega_l + i\,\omega}\right], \tag{2.11}$$

where the anelastic coefficients $Y_l^{\bar{M}}$ and averaged unrelaxed modulus $\bar{M}_U$ replace the anelastic coefficients Y_l^M and unrelaxed modulus M_U, respectively, in relation (2.9). The question is how to determine $Y_l^{\bar{M}}$ and $\bar{M}_U$ for the averaged medium. The coefficients may be determined from

$$\frac{1}{Q_{\bar{M}}(\omega)} \equiv \frac{\mathrm{Im}\bar{M}(\omega)}{\mathrm{Re}\bar{M}(\omega)} \tag{2.12}$$

similarly as in the case of the smooth heterogeneous medium, see eq. (2.8); we will return to this determination in Sections 4 and 5. Relation $\bar{M}_U = \lim_{\omega\to\infty} \bar{M}(\omega)$ has an important implication: because the averaging of $M(\omega)$ gives in the limit the averaged $\bar{M}_U$, we may obtain $\bar{M}_U$ by averaging applied to M_U.

The two remaining questions are: the spatial averaging itself and determination of the relaxation frequencies ω_l. These questions will be addressed in the section on the orthorhombic viscoelastic medium.

3 THE SPATIAL AVERAGING OF THE ELASTIC MEDIUM FOR A 3-D PROBLEM: THE ORTHORHOMBIC REPRESENTATION

The discrete representation developed by Kristek and Moczo (Moczo *et al.* 2014; Kristek *et al.* 2017) has two important properties: (1) The number of non-zero coefficients in the elasticity matrix is the same as for the isotropic or transversely isotropic media, that is, 9 (considering the matrix symmetry). Consequently, the averaged medium neither changes the structure of calculating stress-tensor components nor increases the number of arithmetic operations. (2) If a grid cell contains a planar interface (between two homogeneous materials) perpendicular to the ξ-axis, then the averaged medium in the cell is the transversely isotropic medium with an axis of symmetry parallel to the ξ-axis.

Though the representation is, obviously, approximate, it is efficient and sufficiently accurate (see Moczo *et al.* 2014; Chaljub *et al.* 2015; Maufroy *et al.* 2015; Kristek *et al.* 2017). Because the representation for the elastic medium makes a part of the representation for the viscoelastic medium presented in this article [a consequence of relation (2.6) valid also in 3-D], we show it here in the concise

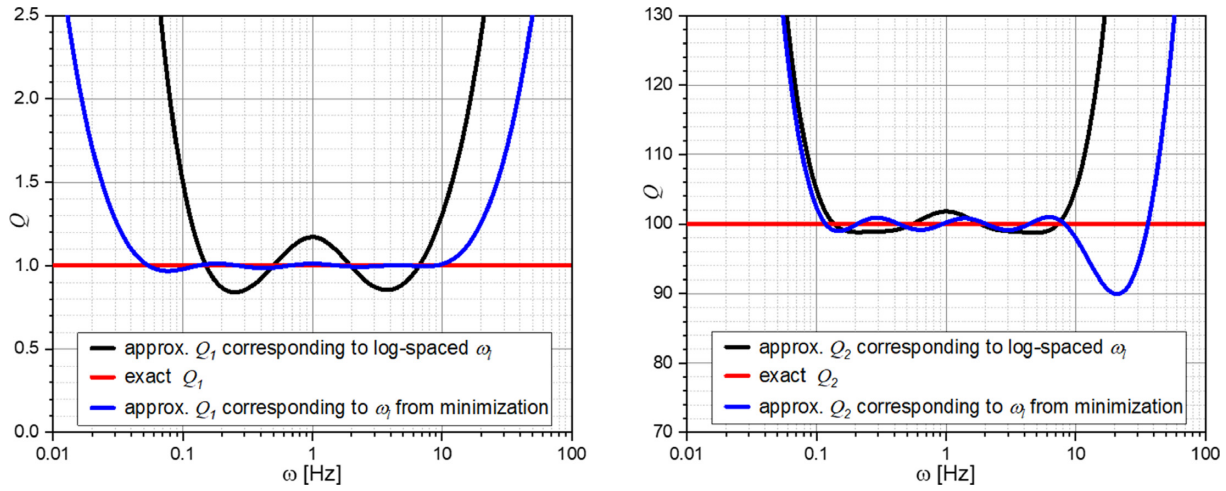

Figure 3. Test 1–red lines: exact $Q_1(\omega) = 1$ and $Q_2(\omega) = 100$, black lines: $Q_1(\omega)$ and $Q_2(\omega)$ approximations corresponding to the log-spaced relaxation frequencies and anelastic coefficients obtained using system of eqs (2.7), blue lines: $Q_1(\omega)$ and $Q_2(\omega)$approximations corresponding to the relaxation frequencies and anelastic coefficients obtained by the minimization approach.

	ω_l	Y_l^{M,Q_1}	Y_l^{M,Q_2}
log-spaced	0.100	-0.0194	0.0133
	0.464	0.1453	0.0095
	2.154	-0.0404	0.0092
	10.000	0.8706	0.0101
minimization	0.105	0.0305	0.0150
	0.716	0.0578	0.0111
	3.447	0.1146	0.0088
	27.055	0.7848	0.0132

Figure 4. Test 2: Comparison of the relaxation frequencies ω_l and anelastic coefficients Y_l^M determined using the log-spaced approach and system of eqs (2.8) with those obtained by the minimization approach explained in Section 5.

form. The stress–strain relation for the averaged medium may be written as

$$\vec{\sigma} = \bar{\mathbf{E}}\,\vec{\varepsilon} \tag{3.1}$$

where the overline indicates the averaged medium, the stress and strain vectors are

$$\begin{aligned}\vec{\sigma} &\equiv \left[\sigma_{xx},\ \sigma_{yy},\ \sigma_{zz},\ \sigma_{xy},\ \sigma_{yz},\ \sigma_{zx}\right]^T,\\ \vec{\varepsilon} &\equiv \left[\varepsilon_{xx},\ \varepsilon_{yy},\ \varepsilon_{zz},\ \varepsilon_{xy},\ \varepsilon_{yz},\ \varepsilon_{zx}\right]^T\end{aligned} \tag{3.2}$$

and the elasticity matrix is

$$\bar{\mathbf{E}} = \begin{bmatrix} \Pi_x & \lambda_{xy} & \lambda_{zx} & 0 & 0 & 0\\ \lambda_{xy} & \Pi_y & \lambda_{yz} & 0 & 0 & 0\\ \lambda_{zx} & \lambda_{yz} & \Pi_z & 0 & 0 & 0\\ 0 & 0 & 0 & 2\mu_{xy} & 0 & 0\\ 0 & 0 & 0 & 0 & 2\mu_{yz} & 0\\ 0 & 0 & 0 & 0 & 0 & 2\mu_{zx} \end{bmatrix} \tag{3.3}$$

For simplicity we omit the overline in the matrix elements. The relation may be also written as

$$\begin{aligned}\sigma_{ij} = \sum_p \Bigg\{ &\sum_q 2\mu_{ij}\,\varepsilon_{pq}\,\delta_{ip}\delta_{jq}\left(1-\delta_{ij}\right)\\ &+ \left[\Pi_i\,\delta_{ip} + \lambda_{ip}\left(1-\delta_{ip}\right)\right]\varepsilon_{pp}\,\delta_{ij}\Bigg\}.\end{aligned} \tag{3.4}$$

The averaged moduli are determined as follows:

$$\mu_{xy} = \langle\langle\mu\rangle^z\rangle^{Hxy} \tag{3.5}$$

$$\Pi_x = \left\langle\left\langle\lambda+2\mu-\frac{\lambda^2}{\lambda+2\mu}\right\rangle^{yz} + \left[\left\langle\frac{\lambda}{\lambda+2\mu}\right\rangle^{yz}\right]^2\langle\lambda+2\mu\rangle^{Hyz}\right\rangle^{Hx} \tag{3.6}$$

$$\begin{aligned}\lambda_{xy} = &\left\langle\left\langle\lambda+2\mu-\frac{\lambda^2}{\lambda+2\mu}\right\rangle^{z} + \left[\left\langle\frac{\lambda}{\lambda+2\mu}\right\rangle^{z}\right]^2\langle\lambda+2\mu\rangle^{Hz}\right\rangle^{Hxy}\\ &\times\left\langle\frac{\left\langle\lambda-\frac{\lambda^2}{\lambda+2\mu}\right\rangle^{z} + \left[\left\langle\frac{\lambda}{\lambda+2\mu}\right\rangle^{z}\right]^2\langle\lambda+2\mu\rangle^{Hz}}{\left\langle\lambda+2\mu-\frac{\lambda^2}{\lambda+2\mu}\right\rangle^{z} + \left[\left\langle\frac{\lambda}{\lambda+2\mu}\right\rangle^{z}\right]^2\langle\lambda+2\mu\rangle^{Hz}}\right\rangle^{xy}.\end{aligned} \tag{3.7}$$

Here, for example $\langle\mu\rangle^z$ means an arithmetic average of μ in the z-direction within the grid cell centred at a grid position at which the average has to be evaluated. $\langle\lambda+2\mu\rangle^{Hz}$ means a harmonic average of $\lambda+2\mu$ in the z-direction within the grid cell centred at a grid position at which the average has to be evaluated. The doubled superscript, for example xy, means an average over the $xy-$cross-section of the grid cell centred at a grid position at which the average has to be evaluated.

The averaged moduli $\{\mu_{yz},\ \mu_{zx}\}$, $\{\Pi_y,\ \Pi_z\}$ and $\{\lambda_{yz},\ \lambda_{zx}\}$ are obtained from eqs (3.5)–(3.7), respectively, using replacements $x \to y$, $y \to z$, $z \to x$. The averaging applies to a volume of the grid cell $h \times h \times h$ centred at a position of the relevant stress-tensor component.

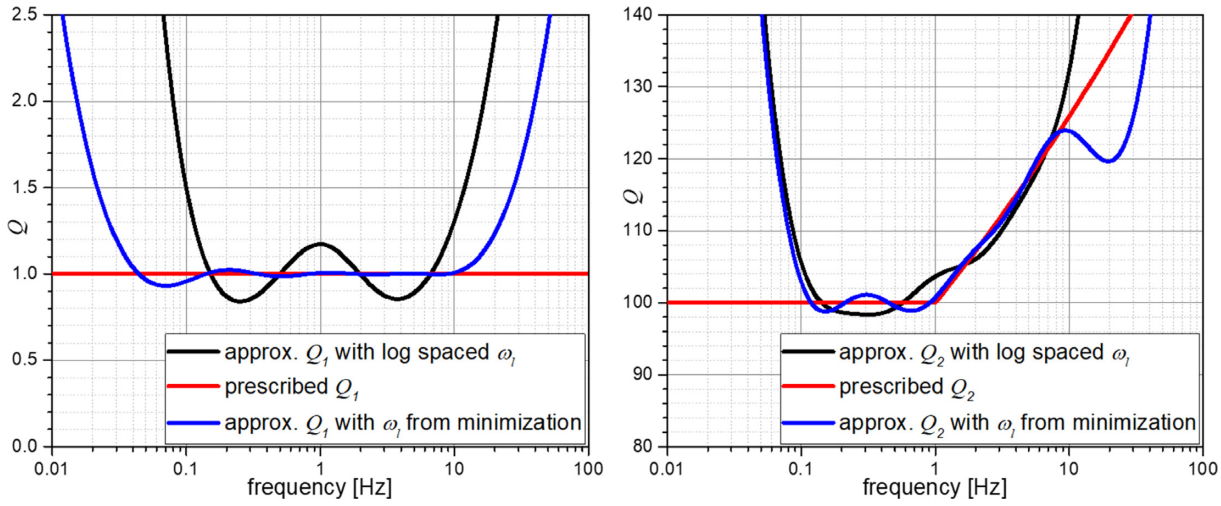

Figure 5. Test 2–red lines: exact $Q_1(\omega)$ and $Q_2(\omega)$, black lines: $Q_1(\omega)$ and $Q_2(\omega)$ approximations corresponding to the log-spaced relaxation frequencies and anelastic coefficients obtained using system of eqs (2.7), blue lines: $Q_1(\omega)$ and $Q_2(\omega)$approximations corresponding to the relaxation frequencies and anelastic coefficients obtained by the minimization approach.

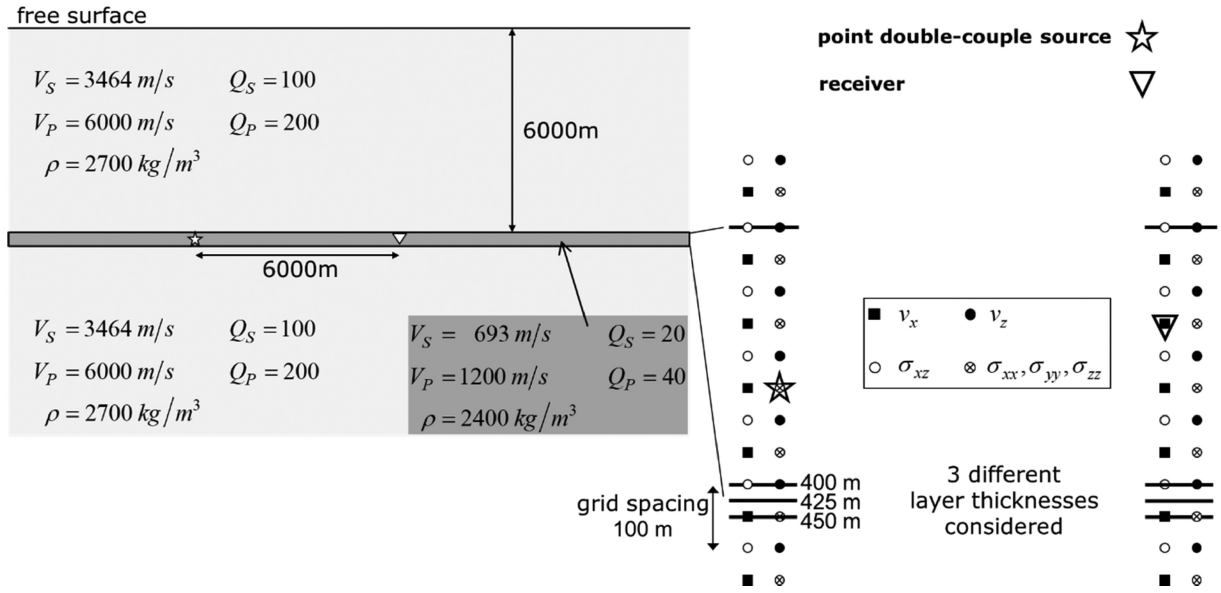

Figure 6. A vertical cross-section of a 3-D problem configuration. The model of medium consists of a horizontal soft layer in a homogeneous half-space. Both point double-couple source and receiver are inside the layer. v_x, v_z—particle-velocity components, σ_{zx}, σ_{xx}, σ_{yy}, σ_{zz}—stress-tensor components.

Because nine elements of the elasticity matrix (3.3) are independent, the averaged medium has an orthorhombic anisotropy with three axes of symmetry that are identical with coordinate axes.

4 ORTHORHOMBIC REPRESENTATION FOR THE VISCOELASTIC MEDIUM

4.1 Stress–strain relation

Analogously to the GMB-EK/GZB time-domain stress–strain relation for 1-D, given by eqs (2.9) and (2.10), the stress–strain relation for 3-D may be written as

$$\vec{\sigma} \;=\; \bar{\mathbf{E}}\,\vec{\varepsilon} \;-\; \sum_{l=1}^{n} \bar{\mathbf{A}}\,\vec{\zeta} \tag{4.1}$$

with stress vector $\vec{\sigma}$, strain vector $\vec{\varepsilon}$ and matrix of averaged unrelaxed moduli $\bar{\mathbf{E}}$ given by eqs (3.2) and (3.3), respectively, and

$$\vec{\zeta} \;\equiv\; \left[\zeta_l^{xx},\ \zeta_l^{yy},\ \zeta_l^{zz},\ \zeta_l^{xy},\ \zeta_l^{yz},\ \zeta_l^{zx}\right]^T \tag{4.2}$$

$$\bar{\mathbf{A}} = \begin{bmatrix} Y_l^{\Pi_x}\Pi_x & Y_l^{\lambda_{xy}}\lambda_{xy} & Y_l^{\lambda_{zx}}\lambda_{zx} & 0 & 0 & 0 \\ Y_l^{\lambda_{xy}}\lambda_{xy} & Y_l^{\Pi_y}\Pi_y & Y_l^{\lambda_{yz}}\lambda_{yz} & 0 & 0 & 0 \\ Y_l^{\lambda_{zx}}\lambda_{zx} & Y_l^{\lambda_{yz}}\lambda_{yz} & Y_l^{\Pi_z}\Pi_z & 0 & 0 & 0 \\ 0 & 0 & 0 & 2Y_l^{\mu_{xy}}\mu_{xy} & 0 & 0 \\ 0 & 0 & 0 & 0 & 2Y_l^{\mu_{yz}}\mu_{yz} & 0 \\ 0 & 0 & 0 & 0 & 0 & 2Y_l^{\mu_{zx}}\mu_{zx} \end{bmatrix}. \tag{4.3}$$

The overline indicates the averaged medium. Again, however, for simplicity we will omit the overline in the matrix elements. An

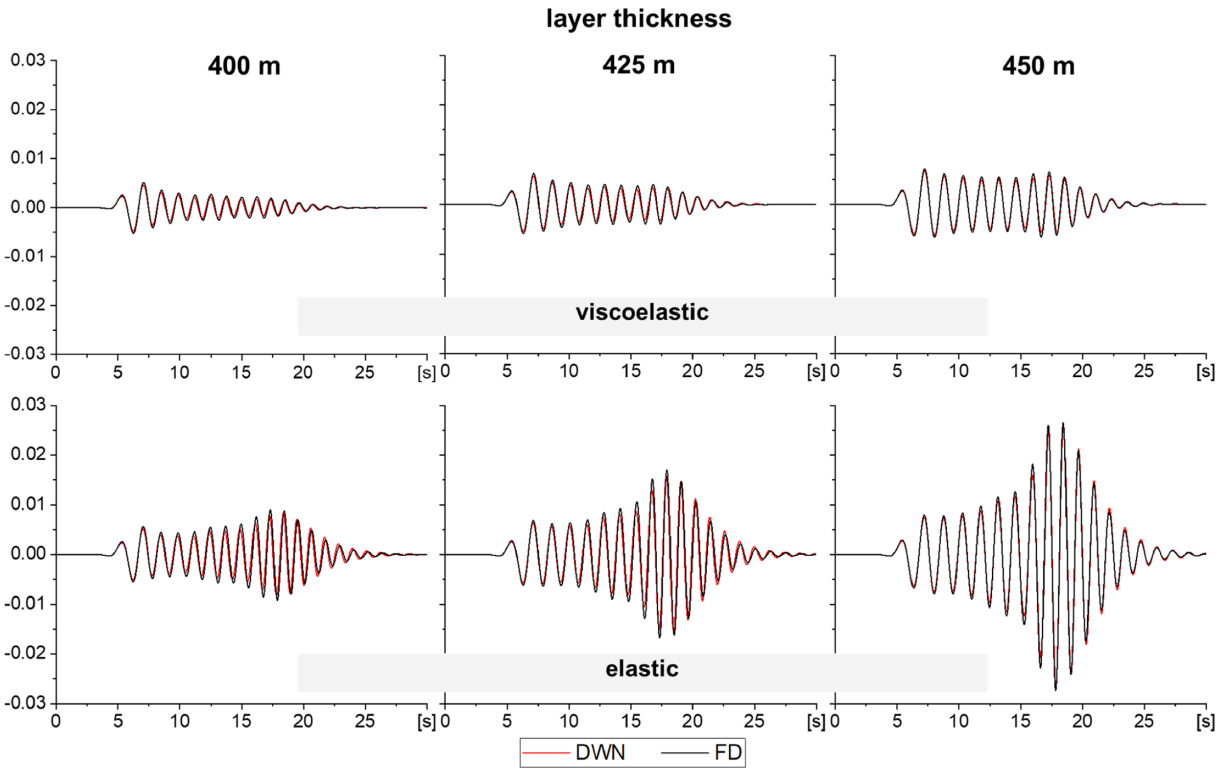

Figure 7. Comparison of the FD seismograms based on the developed discrete representation and DWN seismograms taken as reference for the three layer thicknesses in the model shown in Fig. 6.

alternative form of relation (4.1) is

$$\sigma_{ij} = \sum_p \left\{ \sum_q 2\mu_{ij}\,\varepsilon_{pq}\,\delta_{ip}\,\delta_{jq}\,(1-\delta_{ij}) + \left[\Pi_i\delta_{ip} + \lambda_{ip}\,(1-\delta_{ip})\right]\varepsilon_{pp}\delta_{ij} \right\} - \sum_{l=1}^{n}\sum_p \left\{ \sum_q 2Y_l^{\mu_{ij}}\mu_{ij}\zeta_l^{pq}\delta_{ip}\delta_{jq}\,(1-\delta_{ij}) + \left[Y_l^{\Pi_i}\Pi_i\delta_{ip} + Y_l^{\lambda_{ip}}\lambda_{ip}\,(1-\delta_{ip})\right]\zeta_l^{pp}\delta_{ij} \right\}. \quad (4.4)$$

The anelastic functions obey ordinary differential equations

$$\frac{\partial}{\partial t}\zeta_l^{ij}(t) + \omega_l\zeta_l^{ij}(t) = \omega_l\varepsilon_{ij}(t), \quad l = 1, ..., n, \quad (4.5)$$

where n is the number of relaxation frequencies. Summation convention does not apply to index l in eq. (4.5).

It is obvious that for calculating stress-tensor components in the orthorhombic viscoelastic medium we need to know/determine the unrelaxed moduli μ_{ij}, Π_i and λ_{ij}, anelastic coefficients $Y_l^{\mu_{ij}}$, $Y_l^{\Pi_{ij}}$ and $Y_l^{\lambda_{ij}}$, and relaxation frequencies ω_l. The unrelaxed moduli of the averaged orthorhombic medium are determined by averaging unrelaxed moduli according to eqs (3.5)–(3.7). The anelastic coefficients and relaxation frequencies may be determined jointly in one procedure based on relations between the quality factors and the anelastic coefficients.

4.2 Relations for the anelastic coefficients for the averaged medium

In practice, we know from measurements or we simply estimate quality factors for the P and S waves—$Q_S(\omega)$ and $Q_P(\omega)$. Assume that we know the unrelaxed moduli $\mu = \mu_U$ and $\lambda + 2\mu = \lambda_U + 2\mu_U$ at any point of the medium. (If we do not know them directly, we can determine them from the phase velocities at some reference frequencies—see Moczo *et al.* 2014). Then, at any point of the medium,

$$\mu(\omega) = \mu\left[1 - \sum_{l=1}^{n} Y_l^{\mu}\frac{\omega_l}{\omega_l + i\,\omega}\right] \quad (4.6)$$

with the anelastic coefficients Y_l^{μ} determined from, see eq. (2.8),

$$\frac{1}{Q_S(\omega)} = \frac{\sum_{l=1}^{n} Y_l^{\mu}\frac{\omega_l\,\omega}{\omega_l^2 + \omega^2}}{1 - \sum_{l=1}^{n} Y_l^{\mu}\frac{\omega_l^2}{\omega_l^2 + \omega^2}}, \quad (4.7)$$

Having $\mu(\omega)$, $\mu_{xy}(\omega)$ may be determined according to eq. (3.5) as

$$\mu_{xy}(\omega) = \left\langle\langle\mu(\omega)\rangle^z\right\rangle^{Hxy}, \quad (4.8)$$

where the averaging applies to a volume of the grid cell $h \times h \times h$ centred at a position of the relevant stress-tensor component. Complex values of $\mu_{xy}(\omega)$ are evaluated at a set of reasonably chosen frequencies within the frequency range of interest. The choice of the frequencies will be addressed in Section 5. Consequently, the

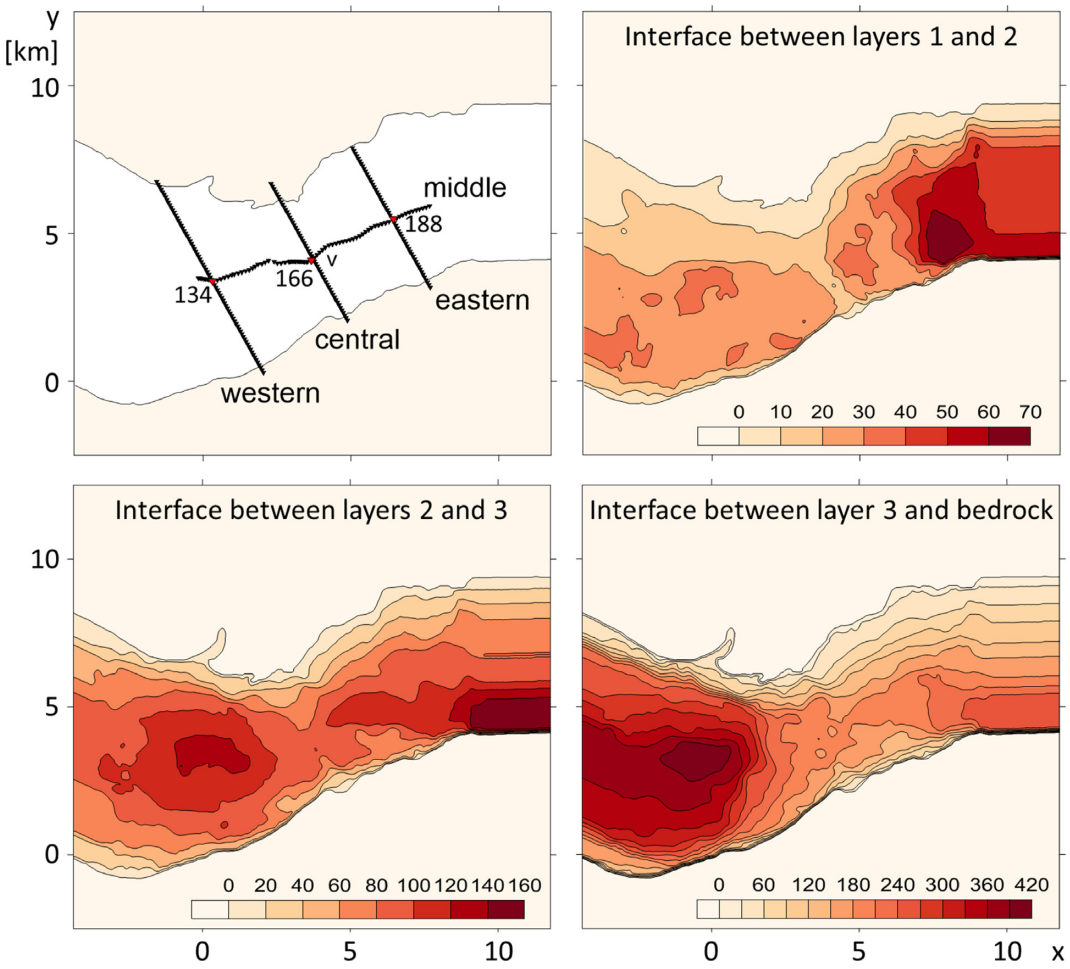

Figure 8. Geometry of the original 3-D model of the Mygdonian basin. Upper left-hand panel: margins of the sedimentary basin at the flat free surface, four horizontal profiles of receivers at the free surface, position of the vertical profile of receivers (v) in the central part of the basin and positions of three selected receivers. Upper right-hand panel: interface between the uppermost and middle sedimentary layers. Lower left-hand panel: interface between the middle and bottom sedimentary layers. Lower right-hand panel: interface between the bottom sedimentary layer and bedrock. (Modified from Kristek *et al.* 2017).

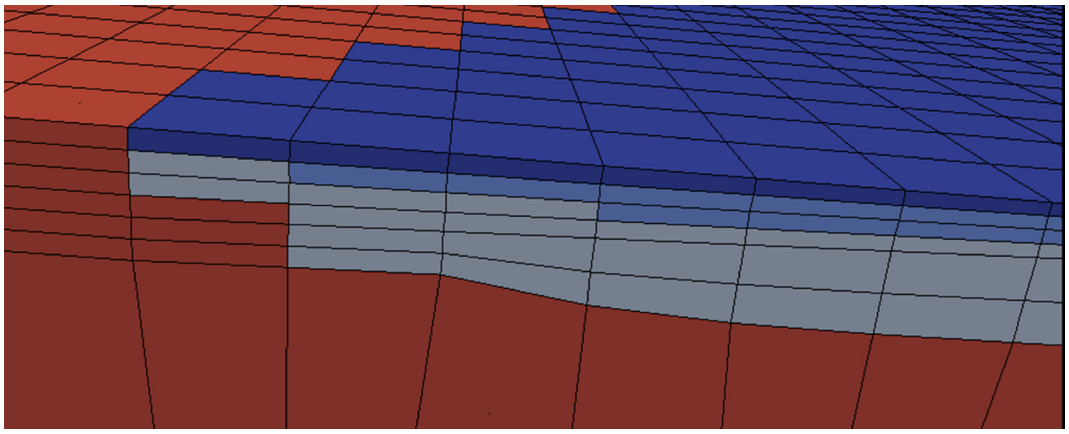

Figure 9. Illustrative detail of the reference SEM model. Different colours represent different homogeneous materials. Element faces exactly follow interfaces. This specific feature makes it possible for SEM to produce sufficiently accurate seismograms. Exactly the same model is considered in the FD simulation. (According to Kristek *et al.* 2017).

Layer	V_S	V_P	ρ	Q_S	Q_κ
	(m/s)	(m/s)	(kg/m^3)		
1	200	1500	2100	20	∞
2	350	1800	2200	35	∞
3	650	2500	2200	65	∞
Bedrock	2600	4500	2600	260	∞

Figure 10. Material parameters of the modified 3-D model of the Mygdonian basin.

anelastic coefficients $Y_l^{\mu_{xy}}$ may be determined from

$$\frac{1}{Q_{\mu_{xy}}(\omega)} \equiv \frac{\mathrm{Re}\mu_{xy}(\omega)}{\mathrm{Im}\mu_{xy}(\omega)} = \frac{\sum_{l=1}^{n} Y_l^{\mu_{xy}} \dfrac{\omega_l\,\omega}{\omega_l^2+\omega^2}}{1-\sum_{l=1}^{n} Y_l^{\mu_{xy}} \dfrac{\omega_l^2}{\omega_l^2+\omega^2}}. \tag{4.9}$$

An analogous procedure applies to $\mu_{yz}(\omega)$ and $\mu_{zx}(\omega)$.
Similarly, at any point of the medium,

$$[\lambda+2\mu](\omega) = (\lambda+2\mu)\left[1-\sum_{l=1}^{n} Y_l^{\lambda+2\mu}\frac{\omega_l}{\omega_l+i\,\omega}\right] \tag{4.10}$$

with $Y_l^{\lambda+2\mu}$ determined from

$$\frac{1}{Q_P(\omega)} = \frac{\sum_{l=1}^{n} Y_l^{\lambda+2\mu} \dfrac{\omega_l\,\omega}{\omega_l^2+\omega^2}}{1-\sum_{l=1}^{n} Y_l^{\lambda+2\mu} \dfrac{\omega_l^2}{\omega_l^2+\omega^2}}. \tag{4.11}$$

Having Y_l^{μ} and $Y_l^{\lambda+2\mu}$, we obtain Y_l^{λ} as

$$Y_l^{\lambda} = \frac{\alpha^2 Y_l^{\lambda+2\mu} - 2\beta^2 Y_l^{\mu}}{\alpha^2-2\beta^2}. \tag{4.12}$$

Consequently we may determine $\lambda(\omega)$:

$$\lambda(\omega) = \lambda\left[1-\sum_{l=1}^{n} Y_l^{\lambda}\frac{\omega_l}{\omega_l+i\,\omega}\right]. \tag{4.13}$$

Having $[\lambda+2\mu](\omega)$ and $\lambda(\omega)$ at any point of the medium, we are ready to evaluate $\Pi_x(\omega)$ according to eq. (3.6) and $Y_l^{\Pi_x}$ from

$$\frac{1}{Q_{\Pi_x}(\omega)} \equiv \frac{\mathrm{Re}\Pi_x(\omega)}{\mathrm{Im}\Pi_x(\omega)} = \frac{\sum_{l=1}^{n} Y_l^{\Pi_x} \dfrac{\omega_l\,\omega}{\omega_l^2+\omega^2}}{1-\sum_{l=1}^{n} Y_l^{\Pi_x} \dfrac{\omega_l^2}{\omega_l^2+\omega^2}}. \tag{4.14}$$

We obtain $Y_l^{\Pi_y}$ and $Y_l^{\Pi_z}$ analogously.
Following Carcione & Cavallini (1995) we calculate the anelastic coefficients $Y_l^{\lambda_{xy}}$, $Y_l^{\lambda_{yz}}$ and $Y_l^{\lambda_{zx}}$ as

$$Y_l^{\lambda_{ij}} = \frac{\Pi_x Y_l^{\Pi_x} + \Pi_y Y_l^{\Pi_y} + \Pi_z Y_l^{\Pi_z}}{3\lambda_{ij}} - 2\frac{\mu_{xy} Y_l^{\mu_{xy}} + \mu_{yz} Y_l^{\mu_{yz}} + \mu_{zx} Y_l^{\mu_{zx}}}{3\lambda_{ij}}. \tag{4.15}$$

5 OPTIMAL PROCEDURE FOR A JOINT DETERMINATION OF THE ANELASTIC COEFFICIENTS AND RELAXATION FREQUENCIES

Several approaches to determine relaxation frequencies and anelastic coefficients have been developed and published after the pioneering articles by Emmerich & Korn (1987) and Carcione *et al.* (1988): for example Robertsson *et al.* (1994); Robertsson (1996); Graves & Day (2003); Asvadurov *et al.* (2004); Liu & Archuleta (2006); van Driel & Nissen-Meyer (2014); Withers *et al.* (2015) and Blanc *et al.* (2016).

Here we present an approach in which we find such relaxation frequencies that are optimal for the whole computational domain, that is, for the whole range of the quality factor values in the model.

Recall relation (2.8):

$$\frac{1}{Q_M(\omega)} = \frac{\sum_{l=1}^{n} Y_l^M \dfrac{\omega_l\omega}{\omega_l^2+\omega^2}}{1-\sum_{l=1}^{n} Y_l^M \dfrac{\omega_l^2}{\omega_l^2+\omega^2}}. \tag{5.1}$$

The relation may be rearranged as

$$\sum_{l=1}^{n} \frac{\omega_l\,\omega+\omega_l^2\,Q_M^{-1}(\omega)}{\omega_l^2+\omega^2}\,Y_l^M = Q_M^{-1}(\omega) \tag{5.2}$$

and

$$1 - \sum_{l=1}^{n} \frac{\omega_l\,\omega\,Q_M(\omega)+\omega_l^2}{\omega_l^2+\omega^2}\,Y_l^M = 0. \tag{5.3}$$

We want to find the relaxation frequencies ω_l and anelastic coefficients Y_l^M satisfying relation (5.3) in the frequency range of interest $[\omega_{\min},\ \omega_{\max}]$. For a reasonably sampled frequency range we may consider an objective function

$$F\left(\omega_l, Y_l^M\right) = \frac{1}{N_\omega-1} \times \sqrt{\sum_{\omega=\omega_{\min}}^{\omega_{\max}} \left(1-\sum_{l=1}^{n} \frac{\omega_l\omega Q(\omega)+\omega_l^2}{\omega_l^2+\omega^2}\,\left|Y_l^M\right|\right)^2}, \tag{5.4}$$

where N_ω is the number of the log-spaced frequencies. Note that this objective function is close to that used by Blanc *et al.* (2016). We use the absolute values of the anelastic coefficients because we look for positive coefficients. We can minimize the function using the Nelder-Mead minimization method. The minimization method could yield the anelastic coefficients and relaxation frequencies for a given spatial position. However, in order to avoid keeping in memory possibly different relaxation frequencies for each grid point, it is computationally significantly more efficient to have the same relaxation frequencies for the whole computational domain. Therefore, we modify the objective function. Instead of the one defined by eq. (5.4), we introduce the objective function as

$$F\left(\omega_l, Y_l^{M,Q_1}, Y_l^{M,Q_2}\right) = \frac{1}{N_\omega-1} \times \sqrt{\sum_{\omega=\omega_{\min}}^{\omega_{\max}} \left(1-\sum_{l=1}^{n} \frac{\omega_l\omega Q_1(\omega)+\omega_l^2}{\omega_l^2+\omega^2}\,\left|Y_l^{M,Q_1}\right|\right)^2} + \frac{1}{N_\omega-1}\sqrt{\sum_{\omega=\omega_{\min}}^{\omega_{\max}} \left(1-\sum_{l=1}^{n} \frac{\omega_l\omega Q_2(\omega)+\omega_l^2}{\omega_l^2+\omega^2}\,\left|Y_l^{M,Q_2}\right|\right)^2}, \tag{5.5}$$

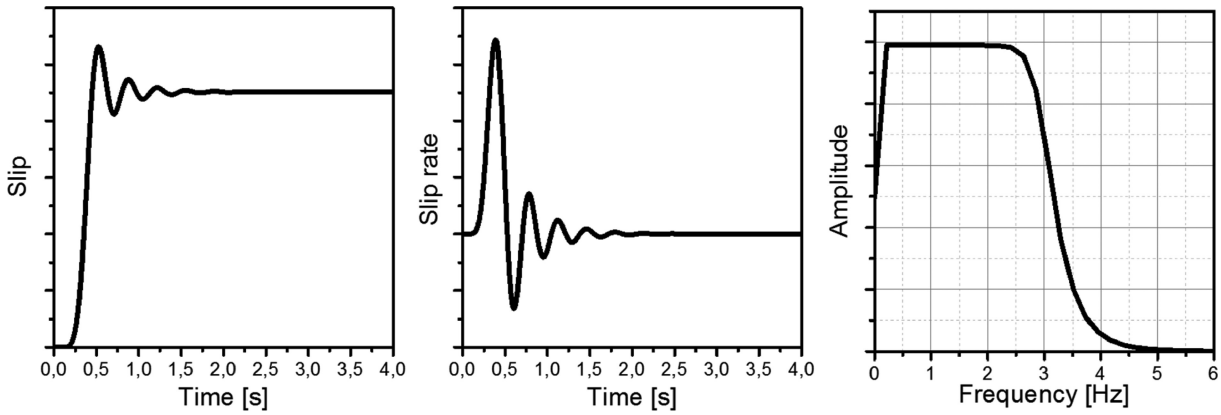

Figure 11. The source time function. Left-hand panel: slip, centre: slip rate, right:-hand panel Fourier amplitude spectrum of the slip rate.

computational domain	16.14 km x 29.31 km x 7.86 km		
number of elements	1 751 040		
polynomial degree	N=4 (5 GLL points per direction)		
number of points (each counted once)	115 605 072		
		vertical	horizontal
(upper) fine mesh	element size	2.5-7.5 m	50 m
	average grid spacing	0.62-1.87 m	12.5 m
	minimum grid spacing	0.43-1.30 m	8.63 m
(lower) coarse mesh	element size	860 m	200 m
	average grid spacing	215 m	50 m
	minimum grid spacing	148.50 m	34.53 m
time step	0.0001 s		
time window	30 s		
note: minimum grid spacing = 0.691 % of average gridsize for N=4			

Figure 12. Computational parameters of the SEM simulation. GLL means Gauss–Lobatto–Legendre.

where $Q_1(\omega)$ and $Q_2(\omega)$ are the most differing $Q(\omega)$ laws in the model. Application of the Nelder-Mead minimization to the objective function (5.5) yields the relaxation frequencies and anelastic coefficients, that is, ω_l, Y_l^{M,Q_1}, Y_l^{M,Q_2}; $l = 1, \ldots, n$. Using the determined relaxation frequencies we could use the Nelder-Mead minimization for finding anelastic coefficients for other $Q(\omega)$ laws in the model of the medium. We checked, however, that we would obtain anelastic coefficients very close to those that we could obtain more efficiently using the determined relaxation frequencies by the least-square method applied to system of eq. (2.8). Therefore we apply the latter simpler approach.

The combination of the Nelder-Mead minimization with the objective function (5.5) provides a sufficiently robust and efficient method for determining the relaxation frequencies and anelastic coefficients. In the next section we present numerical tests illustrating the approach and that it is sufficient to use only two (most differing) $Q(\omega)$ laws in the model of the medium in order to well represent the whole model.

6 NUMERICAL VERIFICATION

6.1 Test of the optimal minimization

Test 1

Assume that two most differing $Q(\omega)$ laws in the model of a medium (one, e.g. in surface sediments, the other in an underlying rock) are $Q_1(\omega) = 1$ and $Q_2(\omega) = 100$, respectively. Obviously, the Q assumed in sediments is extremely low but it can be considered as a stringent value for the testing purposes. Let $[\omega_{\min} = 0.1Hz,\ \omega_{\max} = 10.0Hz]$ be the frequency range in which we want to sufficiently accurately approximate both $Q(\omega)$ laws.

fine grid	size	1585 x 1475 x 59
	grid spacing	10 m
	PML zone	55 grid planes
coarse grid	size	145 x 135 x 140
	grid spacing	110 m
	PML zone	5 grid planes
time step		0.001 s
time window		30 s

Figure 13. Computational parameters of the FDM simulation.

In the approach suggested by Emmerich & Korn (1987) and applied then by many, the frequency range is sampled by log-spaced relaxation frequencies. Kristek & Moczo (2003) suggested four frequencies in their coarse spatial distribution of the material-independent anelastic functions. Following this approach, we may consider $\omega_l \in \{0.1,\ 0.464,\ 2.154, 10.0\}$. For determining anelastic coefficients Y_l^{M,Q_1} , Y_l^{M,Q_2} ; $l = 1, ..., 4$ we may sample both $Q(\omega)$ laws at, for example the seven log-spaced frequencies $\tilde{\omega}_k \in \{0.1,\ 0.2154,\ 0.464,\ 0.99966,\ 2.154,\ 4.641, 10.0\}$ in the considered frequency range of interest. Then we can determine the anelastic coefficients separately for each of the two considered $Q(\omega)$ laws using the least-square method applied to system of eqs (2.8).

Alternatively, we may determine the relaxation frequencies and anelastic coefficients using the method explained in Section 5.

Fig. 2 compares the relaxation frequencies and anelastic coefficients determined by the two alternative approaches. In the approach explained in Section 5 we used 5000 frequencies to sample $Q(\omega)$ laws in the frequency range of interest. We may notice that the standard log-spaced approach yields two negative anelastic coefficients for the $Q_1(\omega) = 1$ law whereas our minimization approach yields only positive values. Fig. 3 shows the exact $Q_1(\omega) = 1$ and $Q_2(\omega) = 100$(red lines), $Q_1(\omega)$ and $Q_2(\omega)$ approximations corresponding to the log-spaced relaxation frequencies and anelastic coefficients obtained using system of eqs (2.8) (black lines), and $Q_1(\omega)$ and $Q_2(\omega)$ approximations corresponding to the relaxation frequencies and anelastic coefficients obtained using the minimization approach (blue lines).

Test 2

In this test two most differing $Q(\omega)$ laws in the model of a medium are $Q_1(\omega) = 1$, and $Q_2(\omega) = 100$; $\omega \in [0, 1]Hz$, $Q_2(\omega) = 100\,\omega^{0.1}$; $\omega \in [1, \infty]Hz$, respectively. As in Test 1 we determine the relaxation frequencies and anelastic coefficients using both approaches. The results are compared in Figs 4 and 5. Fig. 4 compares the relaxation frequencies and anelastic coefficients. We may notice that the standard log-spaced approach yields the same anelastic coefficients for the $Q_1(\omega) = 1$ as in Test 1. The minimization approach yields for the same $Q_1(\omega) = 1$ a little bit different anelastic coefficients compared to those determined in Test 1. This is because the coefficients also depend on the $Q_2(\omega)$ law which differs from that in Test 1. Fig. 5 shows the exact $Q_1(\omega)$ and $Q_2(\omega)$ laws (red lines), $Q_1(\omega)$ and $Q_2(\omega)$ approximations corresponding to the log-spaced relaxation frequencies and anelastic coefficients obtained using system of eqs (2.8) (black lines), and $Q_1(\omega)$ and $Q_2(\omega)$ approximations corresponding to the relaxation frequencies and anelastic coefficients obtained using the minimization approach (blue lines).

In both Test1 and Test 2 the approximations of $Q(\omega)$ laws obtained with the proposed optimization approach are better than those obtained using the log-spaced relaxation frequencies and anelastic coefficients determined by system of eqs (2.8).

6.2 Attenuation of intensive waves in a soft layer

Fig. 6 shows a vertical cross-section of a 3-D problem configuration. The model of medium is made of a horizontal soft layer in a homogeneous half-space. Both layer and half-space are characterized by *P*-wave and *S*-wave speeds and densities corresponding to unrelaxed elastic moduli as well as frequency-independent quality factors for *P* and *S* waves. Note the large contrasts of the speeds and quality factors in the layer and half-space. We consider three variants of the configuration differing from each other by the position of the lower layer-half-space interface and thus also by the layer thickness. The lower layer-half-space interface of the 400-m-thick layer goes through grid positions of the *z*-component of the particle velocity and *zx*-component of the stress tensor. The lower layer-half-space interface of the 450-m-thick layer goes through grid positions of the component of the particle velocity and normal components of the stress tensor. Finally, the lower layer-half-space interface of the 452-m-thick layer is located just in the middle position, that is, one quarter of the grid spacing beneath the grid plane going through the *z*-component of the particle velocity and *zx*-component of the stress tensor. We choose the three variants in order to demonstrate the subcell resolution of the developed discrete representation of heterogeneity of the viscoelastic medium. A point double-couple source as well as a receiver are located inside the soft layer. Their positions inside the layer together with large contrasts of the *P*- and *S*-wave speeds and quality factors imply relatively intensive waves propagating inside the layer. At the same time, relatively low values of the quality factors in the layer imply considerable attenuation of the waves. Altogether we have a configuration for a stringent test of accuracy of the developed discrete representation.

Fig. 7 compares seismograms (*x*-component of the particle velocity) calculated using the finite-difference (FD) and discrete-wavenumber (DWN) methods. In the FD velocity–stress staggered-grid scheme 4th-order accurate in space, 2nd-order accurate in time, effective grid elastic and viscoelastic material parameters are determined according to the discrete representation explained in Sections 3–5. The very accurate DWN simulations, taken here as reference solution, are performed using computer code Axitra (Coutant 1989) based on theory by Bouchon (1981). The lower panel compares the FD and DWN seismograms for the three models with different layer thickness (due to different grid positions of the lower layer–half-space interface). For this comparison we assumed perfectly elastic medium. The upper panel compares the FD and DWN seismograms analogously but for the viscoelastic medium. We can see

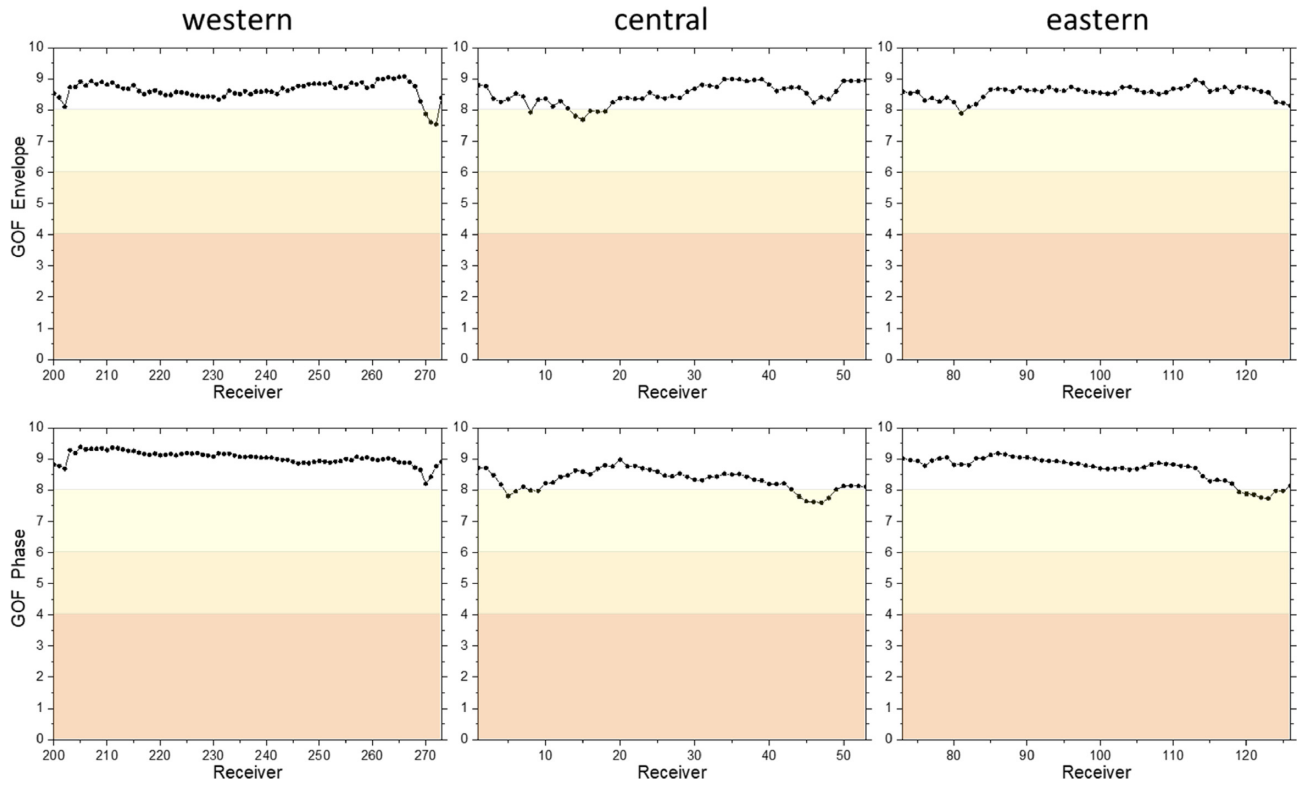

Figure 14. The single-valued envelope and phase GOFs (goodness-of-fit) between the reference SEM seismograms and FDM seismograms along the western, central and eastern receiver profiles.

very good level of agreement between the FD and DWN seismograms confirming accuracy and also subcell resolution of the developed discrete representation of interface between two viscoelastic media.

6.3 Example for the Mygdonian basin model

For the numerical testing of the orthorhombic representation in the perfectly elastic media Kristek *et al.* (2017) developed a special modification of the available realistic 3-D model of the Mygdonian basin near Thessaloniki, Greece. The original model of the Mygdonian basin is shown in Fig. 8. The geometry of material interfaces was modified so that the element faces exactly follow interfaces. This means that the SEM can exactly account for the geometry of material interfaces. Fig. 9 illustrates the SEM mesh. Contact of elements with different colours is a material interface; there are five interfaces in the figure showing a detail of the basin edge. For such a specially modified model the SEM seismograms are adequately accurate and may be considered a reference solution for testing the FD simulation based on the orthorhombic representation. Thus, exactly the same model was considered in the FD simulation. Kristek *et al.* (2017) show very good level of agreement between the SEM and FD solutions.

For the numerical testing of the orthorhombic representation in the viscoelastic media we use the same specially modified elastic model. We just make the model viscoelastic by defining frequency-independent Q factors. Q_S factors are simply defined as $Q_S = V_S/10$ and quality factors for the bulk modulus Q_κ are assumed infinite in each layer and bedrock. Material parameters of the model are shown in Fig. 10. The wavefield is generated by a point double-couple source located at a depth of 5 km. The source time function is shown in Fig. 11. The slip-rate time function is defined as a low-pass filtered Gaussian pulse. The slip is obtained by integrating the slip-rate function.

The reference SEM seismograms are computed using the SPECFEM3D code developed by Komatitsch and Tromp (e.g. Komatitsch and Tromp 1999; Tromp *et al.* 2008; Peter *et al.* 2011). The FD seismograms are computed using the FDSim3D code (Kristek & Moczo 2014; Moczo *et al.* 2014). Figs 12 and 13 summarize the SEM and FD computational parameters.

We calculated the FD seismograms using a spatially discontinuous grid (Kristek *et al.* 2010). Fig. 14 shows the single-valued envelope and phase GOFs (goodness-of-fit) between the reference SEM seismograms and FD seismograms along the western, central and eastern receiver profiles. GOFs are calculated for the entire 30-s window in the frequency range [0.1, 5] Hz from the arithmetic average of the single-valued misfits evaluated separately for each component (Kristekova *et al.* 2009). Recall that GOF larger than 8 means an excellent fit and GOF = 10 means the perfect agreement. Fig. 15 shows the single-valued envelope and phase GOFs for the middle and vertical receiver profiles. It is clear from Figs 14 and 15 that except relatively small number of receivers the fit between the SEM and FD seismograms is excellent.

Fig. 16 compares the SEM and FD seismograms at receivers 134, 166 and 188. In addition to seismograms themselves the figure also shows the time–frequency envelope and phase GOFs between the reference SEM and FD seismograms. Seismograms for each receiver position are absolutely scaled with respect to the maximum amplitude from all components (EW component for receiver 134 and 166, NS component for receiver 188). The GOFs, however, are evaluated individually for each component. This is why GOFs for the vertical component at receiver position 188 are larger than

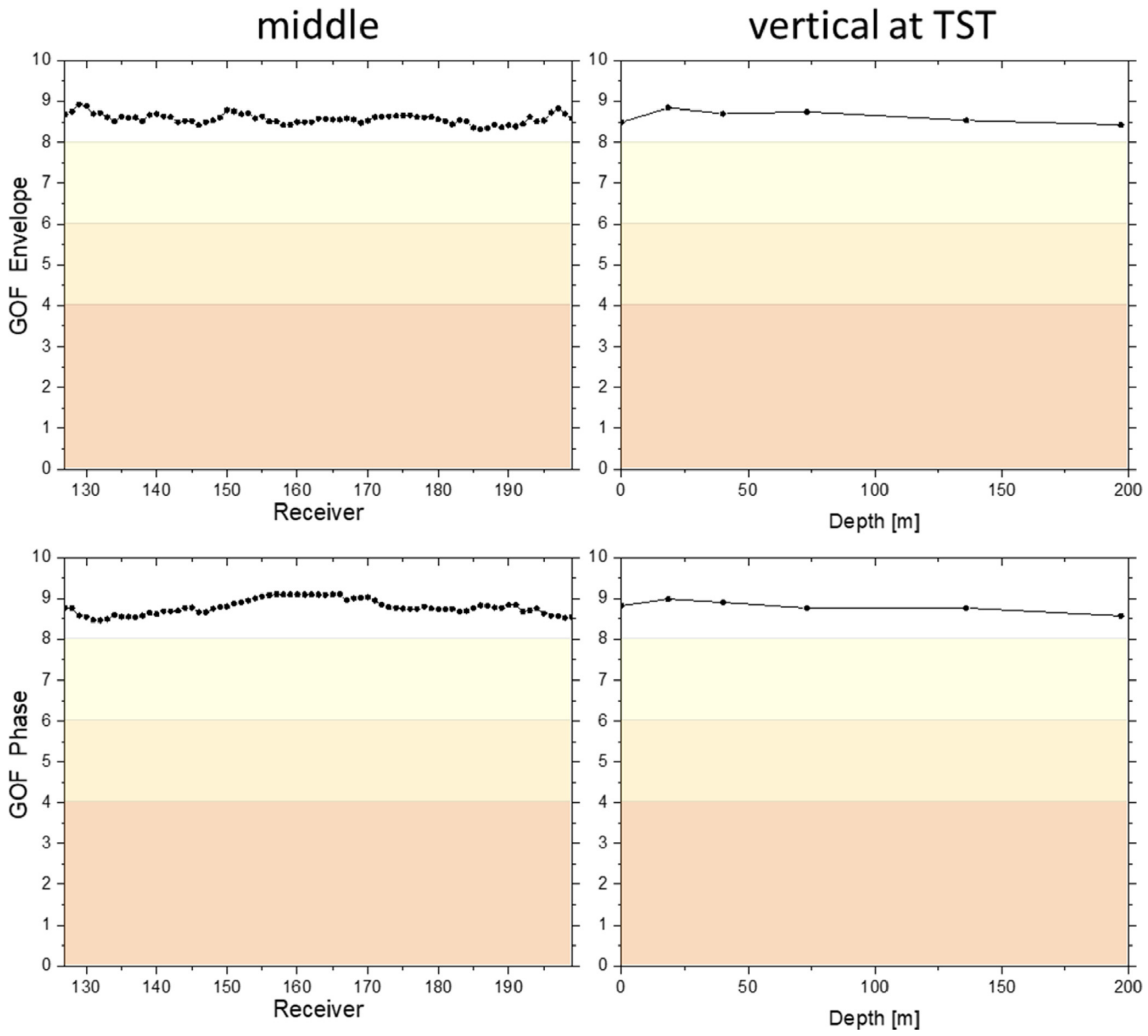

Figure 15. The single-valued envelope and phase GOFs (goodness-of-fit) between the reference SEM seismograms and FDM seismograms along the middle profile and vertical profile.

GOFs for the NS or EW components despite their smaller relative importance. We can see that the level of agreement between the reference SEM and FD seismograms is consistent with the level of agreement quantified by the single-valued GOFs shown in Figs 14 and 15. We may particularly point out the very good agreement between the SEM and FD seismograms in later times.

7 CONCLUSIONS

We have developed a new orthorhombic representation of a heterogeneous viscoelastic medium with interfaces. Heterogeneity of the medium in a FD cell is represented by an averaged medium with an orthorhombic anisotropy with three axes of symmetry that are identical with the coordinate axes. The representation is a generalization of the orthorhombic representation of the heterogeneous elastic medium with interfaces (Kristek *et al.* 2017). Effective material grid parameters are evaluated numerically as volume orthorhombic averages in the grid cells centred at the grid positions of the corresponding stress-tensor components.

We have also found an optimal procedure for a joint determination of the anelastic coefficients and relaxation frequencies for an arbitrary Q(ω) law.

We numerically verified both the optimal procedure and orthorhombic representation. For the latter we used two stringent model-wavefield configurations: 3-D wavefields in a soft internal layer in a half-space and a complex model of the Mygdonian sedimentary basin.

For the layer model we compared FD seismograms with seismograms calculated using the DWN method. The FD seismograms are in excellent agreement with the DWN seismograms.

The 3-D model of the Mygdonian basin was specially designed. In the original model, geometry of the material interfaces was modified so that the element faces exactly follow interfaces. This made it possible to achieve sufficient accuracy with the SEM. The SE seismograms can be thus considered as reference. The FD seismograms were obtained using a discontinuous grid consisting of the fine and coarse uniform grids for the same geometry of interfaces as in the SE model. For quantitative comparison of the FD and SE seismograms we evaluated goodness-of-fit in envelope and phase at several hundreds receivers. The FD and SE seismograms are in excellent fit for a vast majority of receivers. At several receivers the fit is very good.

Both verification tests demonstrated a very good accuracy and subcell resolution of the developed representation.

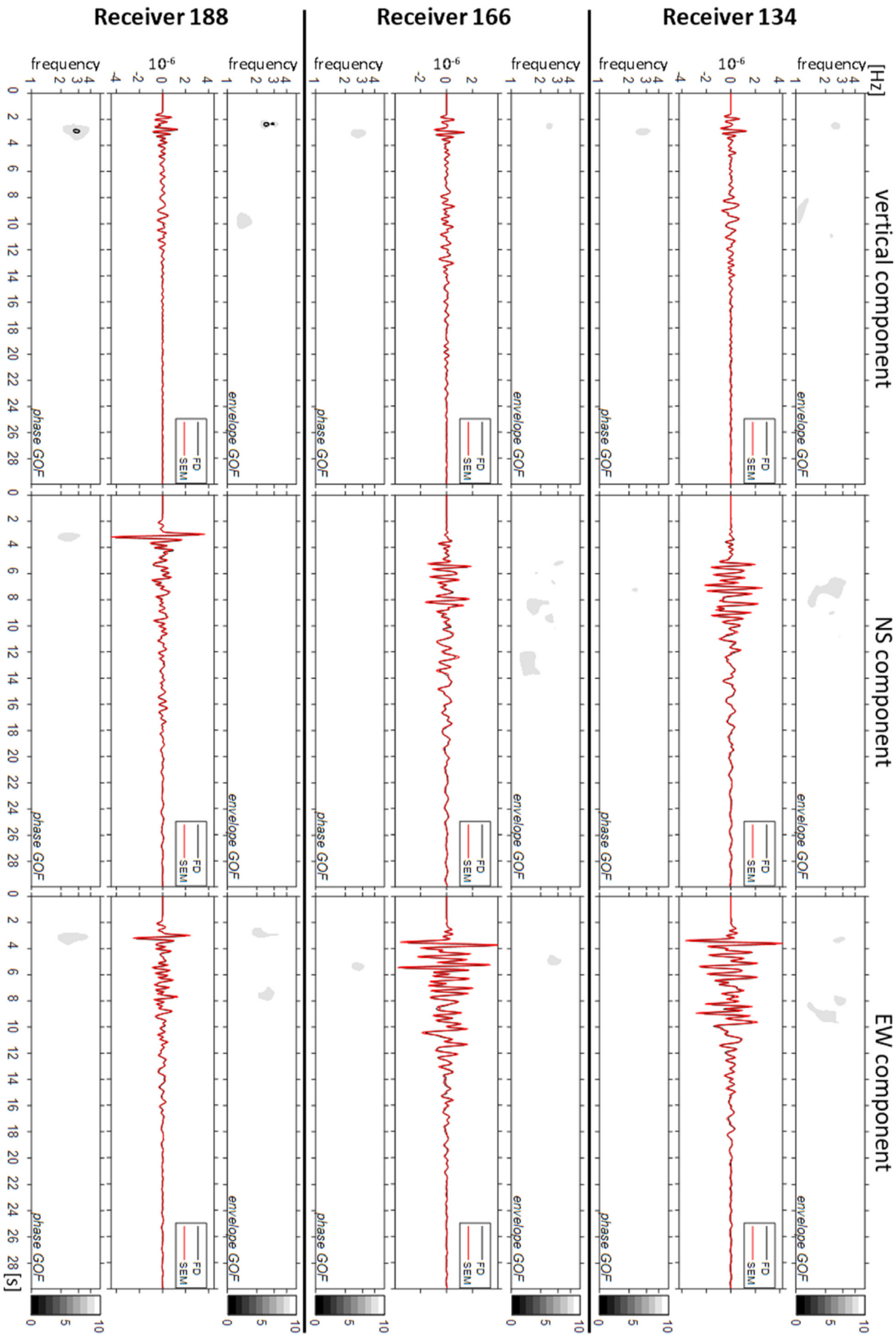

Figure 16. Comparison of the FD seismograms with the reference SEM seismograms for receivers 134, 166 and 188.

The orthorhombic representation neither changes the structure of calculating stress-tensor components nor increases the number of arithmetic operations compared to a smooth weakly heterogeneous viscoelastic medium. The orthorhombic representation is applicable to modelling seismic wave propagation and earthquake motion in isotropic models with material interfaces and smooth

heterogeneities using velocity–stress, displacement–stress and displacement FD schemes on staggered, partly staggered, Lebedev and collocated grids.

ACKNOWLEDGEMENTS

This work was supported by the Slovak Research and Development Agency under the contract APVV-15–0560 (project ID-EFFECTS). Part of the calculations were performed in the Computing Centre of the Slovak Academy of Sciences using the supercomputing infrastructure acquired in project ITMS 26230120002 and 26210120002 (Slovak infrastructure for high-performance computing) supported by the Research & Development Operational Programme funded by the ERDF. This work was also partially supported by the Slovak Foundation Grant VEGA-2/0188/15.

REFERENCES

Asvadurov, S., Knizhnerman, L. & Pabon, J., 2004. Finite-difference modeling of viscoelastic materials with quality factors of arbitrary magnitude, *Geophysics,* **69**(3), 817–824.

Blanc, E., Komatitsch, D., Chaljub, E., Lombard, B. & Xie, Z., 2016. Highly accurate stability-preserving optimization of the Zener viscoelastic model, with application to wave propagation in the presence of strong attenuation, *Geophys. J. Int.,* **205,** 427–439.

Bouchon, M., 1981. A simple method to calculate Green's functions for elastic layered media, *Bull. seism. Soc. Am.,* **71,** 959–971.

Carcione, J.M., 2015. *Wave Fields in Real Media: Wave Propagation in Anisotropic, Anelastic, Porous and Electromagnetic Media,* 3rd edn, Elsevier.

Carcione, J.M. & Cavallini, F., 1995. Attenuation and quality factor surfaces in anisotropic-viscoelastic media, *Mech. Mat.,* **19,** 311–327.

Carcione, J.M., Kosloff, D.D. & Kosloff, R., 1988. Wave-propagation simulation in a linear viscoelastic medium, *Geophys. J.,* **95,** 597–611.

Chaljub, E. *et al.*, 2015. 3D numerical simulations of earthquake ground motion in sedimentary basins: testing accuracy through stringent models, *Geophys. J. Int.,* **201,** 90–111.

Chaljub, E., Moczo, P., Tsuno, S., Bard, P.-Y., Kristek, J., Käser, M., Stupazzini, M. & Kristekova, M., 2010. Quantitative comparison of four numerical predictions of 3D ground motion in the Grenoble Valley, France, *Bull. seism. Soc. Am.,* **100**(4), 1427–1455.

Coutant, O., 1989. Program of numerical simulation Axitra, *Res. Rep. LGIT (in French),* Université Joseph Fourier, Grenoble.

Day, S.M., 1998. Efficient simulation of constant Q using coarse-grained memory variables, *Bull. seism. Soc. Am.,* **88**(4), 1051–1062.

Day, S.M. & Minster, J.B., 1984. Numerical simulation of wavefields using a Padé approximant method, *Geophys. J. R. astr. Soc.,* **78**(1), 105–118.

Emmerich, H. & Korn, M., 1987. Incorporation of attenuation into time-domain computations of seismic wave fields, *Geophysics,* **52,** 1252–1264.

Graves, R.W. & Day, S.M., 2003. Stability and accuracy analysis of coarse-grain viscoelastic simulations, *Bull. seism. Soc. Am.,* **93,** 283–300.

Komatitsch, D. & Tromp, J., 1999. Introduction to the spectral-element method for 3-D seismic wave propagation, *Geophys. J. Int.,* **139,** 806–822.

Kristek, J. & Moczo, P., 2003. Seismic-wave propagation in viscoelastic media with material discontinuities: A 3D fourth-order staggered-grid finite-difference modelling, *Bull. seism. Soc. Am.,* **93**(5), 2273–2280.

Kristek, J. & Moczo, P., 2014. FDSim3D – The Fortran95 Code for Numerical Simulation of Seismic Wave Propagation in 3D Heterogeneous Viscoelastic Media. www.cambridge.org/moczo.

Kristek, J., Moczo, P., Chaljub, E. & Kristekova, M., 2017. An orthorhombic representation of a heterogeneous medium for the finite-difference modelling of seismic wave propagation, *Geophys. J. Int.,* **208,** 1250–1264.

Kristek, J., Moczo, P. & Galis, M., 2010. Stable discontinuous staggered grid in the finite-difference modelling of seismic motion, *Geophys. J. Int.,* **183**(3), 1401–1407.

Kristekova, M., Kristek, J. & Moczo, P., 2009. Time-frequency misfit and goodness-of-fit criteria for quantitative comparison of time signals, *Geophys. J. Int.,* **178,** 813–825.

Liu, P. & Archuleta, R.J., 2006. Efficient modeling of Q for 3D numerical simulation of wave propagation, *Bull. seism. Soc. Am.,* **96**(4A), 1352–1358.

Liu, H.-P., Anderson, D.L. & Kanamori, H., 1976. Velocity dispersion due to anelasticity; implications for seismology and mantle composition, *Geophys. J. R. astr. Soc* **47,** 41–58.

Maufroy, E. *et al.*, 2015. Earthquake ground motion in the Mygdonian basin, Greece: the E2VP verification and validation of 3D numerical simulation up to 4 Hz, *Bull. seism. Soc. Am.,***105**(3), 1398–1418.

Moczo, P., Gregor, D., Kristek, J. & de la Puente, J., 2018. A discrete representation of material heterogeneity for the finite-difference modelling of seismic wave propagation in a poroelastic medium, *Geophys. J. Int.,* doi:10.1093/gji/ggy412.

Moczo, P. & Kristek, J., 2005. On the rheological models used for time-domain methods of seismic wave propagation, *Geophys. Res. Lett.,* **32,** L01306, doi:10.1029/2004GL021598

Moczo, P., Kristek, J. & Galis, M., 2014. *The Finite-Difference Modelling of Earthquake Motions: Waves and Ruptures,* Cambridge University Press.

Moczo, P., Kristek, J., Vavryčuk, V., Archuleta, R.J. & Halada, L., 2002. 3D heterogeneous staggered-grid finite-difference modeling of seismic motion with volume harmonic and arithmetic averaging of elastic moduli and densities, *Bull. seism. Soc. Am.,* **92**(8), 3042–3066.

Peter, D. *et al.*, 2011. Forward and adjoint simulations of seismic wave propagation on fully unstructured hexahedral meshes, *Geophys. J. Int.,* **186,** 721–739.

Petersson, N.A. & Sjögreen, B., 2012. Stable and efficient modeling of anelastic attenuation in seismic wave propagation, *Commun. Computat. Phys.,* **12,** 193–225.

Robertsson, J.O.A., 1996. A numerical free-surface condition for elastic/viscoelastic finite-difference modeling in the presence of topography, *Geophysics,* **61**(6), 1921–1934.

Robertsson, J.O.A., Blanch, J.O. & Symes, W.W., 1994. Viscoelastic finite-difference modeling, *Geophysics,* **59**(9), 1444–1456.

Tromp, J., Komatitsch, D. & Liu, Q., 2008. Spectral-element and adjoint methods in seismology, *Commun. Comput. Phys.,* **3,** 1–32.

van Driel, M. & Nissen-Meyer, T., 2014. Optimized viscoelastic wave propagation for weakly dissipative media, *Geophys. J. Int.,* **199**(2), 1078–1093.

Withers, K.B., Olsen, K.B. & Day, S.M., 2015. Memory-efficient simulation of frequency-dependent Q, *Bull. seism. Soc. Am.,* **105**(6), 3129–3142.

Yang, P., Brossier, R., Métivier, L. & Virieux, J., 2016. A review on the systematic formulation of 3-D multiparameter full waveform inversion in viscoelastic medium, *Geophys. J. Int.,* **207**(1), 129–149.